Hydrophobic coating- and surface active solvent-mediated self-assembly of charged gold and silver nanoparticles at water–air and water–oil interfaces†

Lijun Xu,[a] Guobin Han,[b] Jiawen Hu,*[a] Yan He,[a] Jiangao Pan,[a] Yongjun Li*[a] and Jiannan Xiang[a]

Received 25th November 2008, Accepted 30th March 2009
First published as an Advance Article on the web 18th May 2009
DOI: 10.1039/b820970g

We report self-assembly of charge-stabilized gold and silver nanoparticles at water–air and water–oil interfaces, *via* manipulation of the interactions between the interfaces and the adsorbing nanoparticles. Nanoparticle adsorption from bulk colloids to an interface is an energy-favored, but finite sorption barrier-restrained (kinetics-controlled) process. Consequently, to successfully mediate self-assembly of nanoparticles, the finite sorption barrier should be decreased. That can be accomplished by manipulating its three controlling forces: the repulsive electrostatic force, the repulsive van der Waals force, and the attractive hydrophobic force between the interface and the adsorbing nanoparticles. It was found that hydrophobic coatings change nanoparticle hydrophobicity and greatly increase the attractive hydrophobic force. Surface active organic solvents (methanol, ethanol, isopropanol, and acetone) decrease the attractive hydrophobic force to some extent. However, they decrease the repulsive electrostatic force to a larger extent, *via* a "charge dilution" mechanism, due to their positive adsorption at the charged water–air and water–oil interfaces. Hydrophobic coatings and organic solvents consequently decrease the sorption barrier, facilitate nanoparticles overcoming the sorption barrier, and mediate the self-assembly of nanoparticles.

Introduction

Organization of nanoparticles into thin films is an important step toward harnessing the novel properties of individual nanoparticles, and provides options for designing and optimizing material properties.[1] Among a wide variety of strategies, liquid–air and liquid–liquid interfaces have emerged as an ideal platform for self-assembly of nanoparticles.[2,3] Much progress in this direction has been achieved *via in situ* interface reduction,[4–6] the Langmuir–Blodgett method,[7] electrostatic and π–π interactions,[8,9] voltage-induction[10] and so forth. Hierarchical self-assembly of ligand-stabilized nanoparticles at fluid interfaces was recently reported, where thermal fluctuations compete with interfacial energy and give rise to particle size-dependent self-assembly.[11]

Over the past few years increasing effort has been directed toward assembly of pre-formed, charge-stabilized nanoparticles at liquid–air and liquid–liquid interfaces.[12–23] Charged nanoparticles provide more options, compared with ligand-stabilized, uncharged nanoparticles, for post-modification of their surface properties, and thus for regulating the interactions that control the assembly process. Most reported methods enable assembly by manipulating particle hydrophobicity.[12–18] We reported previously that electrolytes can salt out citrate-reduced silver nanoparticles at the water–air interface, and enable their aggregation therein without the aid of surfactants.[19] Jin *et al.* prepared similar fractal aggregates of silver/gold roughened core-shell nanoparticles at the water–air interface, using a thermoaccelerated electroless plating method.[20] Very recently, Reincke *et al.*[21] and Li *et al.*[22] found that ethanol can drive hydrophilic nanoparticles to a water–oil interface to form nanoparticle films. Huo *et al.* reported that Fe_2O_3 nanoparticles can spontaneously form a monolayer at a water–air interface, by leaving the aqueous colloids undisturbed.[23]

When nanoparticles adsorb from bulk colloids to the liquid–air or liquid–liquid interfaces, they spontaneously form monolayers without guidance or management from an outside source, which is known as the term self-assembly. Paunov *et al.*[24] and Reincke *et al.*[25] have proposed general thermodynamic mechanisms for understanding the assembly of micrometer and nanometer particles, respectively. Other authors have well studied the behavior of colloidal particles already adsorbed at the interfaces. For the readers who are interested, some recent papers are highly recommended.[26] To date, however, relatively limited attention has been paid to nanoparticle adsorption. The nanoparticle adsorption process

[a] *State Key Laboratory for Chemo/Biosensing and Chemometrics, Biomedical Engineering Center, and College of Chemistry and Chemical Engineering, Hunan University, Changsha, 410082, China. E-mail: jwhu@hnu.cn, liyje@hnu.cn; Fax: +86-0731-8821740*
[b] *State Key Laboratory for Physical Chemistry of Solid Surfaces and Department of Chemistry, Xiamen University, Xiamen, 361005, China*

† Electronic supplementary information (ESI) available: Scheme for preparation and transfer of the nanoparticle films, contact angle measurements on Au films and zeta potential correction. See DOI: 10.1039/b820970g

serves as a mass transfer process, and is thus prerequisite for the subsequent self-assembly of nanoparticles at the interfaces. For that reason, our aim was to elucidate the influence of a variety of mediators (salt, hydrophobic coating, and organic solvents) on the interactions between interfaces and adsorbing particles that kinetically control nanoparticle adsorption. Because the role of salt in nanoparticle adsorption process has been revealed in our previous paper,[19] the present study focuses mainly on hydrophobic coating- and organic solvent-mediated interface assembly. In this report, we will preliminarily reveal the mechanism of hydrophobic coating-mediated self-assembly of nanoparticles. Furthermore, we propose a "charge dilution" mechanism to understand ethanol-mediated self-assembly of nanoparticles, and then generalize the role of ethanol to surface-active organic solvents.

Materials and methods

$HAuCl_4$, $AgNO_3$, trisodium citrate, anhydrous methanol, anhydrous ethanol, isopropanol, acetone, pentane, *n*-hexane, cyclohexane and toluene, all of analytical grade, were purchased from Sinopharm Chemical Reagent Co. Ltd. and used as received. Mercaptoacetic acid was obtained from Aldrich. Water purified with a Milli-Q system was used throughout the study.

Silver and gold nanoparticles with average sizes of 12 and 40 nm were prepared by citrate reduction.[27,28] The scheme for preparation and transfer of the nanoparticle films is given in the ESI.† Briefly, nanoparticle films supported at water–air and water–oil interfaces were prepared by rapidly adding up to 2 mL of organic solvent (methanol, ethanol, isopropanol or acetone) to 5 mL of colloids without and with <5 mL of an oil phase (pentane, *n*-hexane, cyclohexane or toluene), respectively. After adding the organic solvent, the colloid–air or colloid–oil system was left undisturbed. Nanoparticle films formed at the water–air interface in a few minutes to a few hours, and at the water–oil interface even during addition of the organic solvent. Once nanoparticle films were formed, most of the oil phase was removed by syringe from the top of the container. Evaporation of the remaining oil shrank the nanoparticles at the interface.

UV-Vis spectra were measured on a UV2300 spectrophotometer (Tianmei, China) using a 1-cm quartz cell. The nanoparticle films formed at water–air and water–hexane interfaces were transferred to a clean Si(100) wafer for scanning electron microscopy (SEM, JSM-6700F, JEOL) characterization. A thin Au layer was evaporated on the nanoparticle films to improve the SEM image sharpness. Surface tension of the water–organic solvent mixtures was measured at 25 ± 1 °C by the Wilhelmy plate method using a Sigma701 tensiometer (KSV Instruments). The influence of organic solvents on particle contact angle was determined approximately by placing a 5 μL drop of the water–organic solvent mixture on vacuum-evaporated Ag and Au films. Contact angles were measured using a JC2000C instrument (Powereach, China). Zeta (ζ) potential measurements of the colloids were conducted at 25 °C using a Zeta Pals potential analyzer (Brookhaven Instruments Co.).

Results and discussion

Formation of nanoparticle films at water–air and water–oil interfaces

Citrate-reduced silver[27] and gold nanoparticles[28] were used to prepare nanoparticle films. Fig. 1 (left) shows an ethanol-free 40 nm Au colloid covered with a hexane layer. It is apparent that a well defined interface separates the pink colloid and the colorless hexane. In Fig. 1 (right) a thin nanoparticle film is clearly visible at the interface after addition of ethanol. The pink colour of the colloid is much less intense than that of the ethanol-free colloid, indicating that most nanoparticles are driven to the interface upon the addition of ethanol. We further observed that very dilute nanoparticle films, although not visible enough, can often be distinguished at the interface even without the addition of ethanol, which indicates the tendency of nanoparticles to adsorb to the interface.

Fig. 2A shows the UV-Vis absorption spectra of the 40 nm colloid samples taken from the lower colloid phases of the colloid–oil diphase systems upon addition of varying amount of ethanol. Consistent with the color fading trend, the intensity of the surface plasmon absorption peak of Au colloids centered at 530 nm gradually decreases with the increase of ethanol amount. This decrease is caused by two reasons: nanoparticle transfer and colloid dilution caused by dissolved ethanol. To quantitatively evaluate the amount of transferred nanoparticles, we added ethanol at the same rate and defined a transfer parameter as $\Delta S_i/S_{r,i} = (S_{r,i} - S_{s,i})/S_{r,i}$, where $S_{s,i}$ and $S_{r,i}$ are the sample and reference integrated areas, respectively. The sample integrated area $S_{s,i}$ is obtained by integrating the surface plasmon absorption peak of Au colloids from the UV-Vis spectrum of the lower colloid phase. Similarly, a reference integrated area $S_{r,i}$ is obtained from the UV-Vis spectrum of the reference colloids, which were prepared by gently adding ethanol (that largely avoids nanoparticle to transfer to the air–water interface, see following discussions) into pure Au colloids. The reference colloids have an identical volume and contain the same amount of dissolved ethanol to the corresponding lower colloid phase in the colloid–oil diphase system. Therefore, the transfer parameter eliminates the colloid dilution effect and represents the proportion of nanoparticles transferred to the interface. Fig. 2B shows the transfer parameter as a function of the added amount of

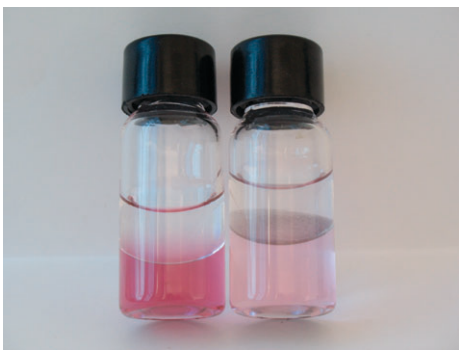

Fig. 1 Digital photograph of a 40 nm gold colloid covered with hexane without (left) and with the addition of 28.6 vol.% of ethanol (right).

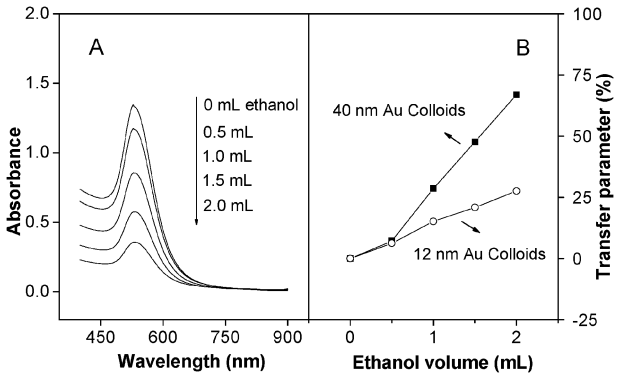

Fig. 2 UV-Vis spectra of the lower 40 nm Au colloid phases (A) and the corresponding proportion of nanoparticles transferred to the interface (B) upon addition of varying amount of ethanol into the colloid–hexane diphase system. 5 mL of colloids and 5 mL of hexane were used to prepare the colloid–hexane diphase system. The proportion of transferred nanoparticles for 12 nm Au colloids is also listed in Fig. 2B for comparison.

ethanol. It is clear that the amount of transferred nanoparticles shows a roughly linear dependence on the added amount of ethanol when the ethanol was added at the same rate. We added at the most 2 mL of ethanol into a 5 mL–5 mL colloid–hexane diphase system, which drove 67% 40 nm nanoparticles and 27.6% 16 nm Au nanoparticles to the water–oil interface. Therefore, the amount of transferred nanoparticles also has a dependence on the particle size. Nanoparticle films at a water–air interface were prepared similarly by rapidly adding ethanol to aqueous colloid in the absence of a hexane layer, then leaving the colloid undisturbed. In contrast to the very fast assembly of nanoparticles at a water–hexane interface, times from a few minutes to a few hours were required for nanoparticle films to form at a water–air interface. Fig. 3a and b show SEM images of silver and 12 nm Au nanoparticle films formed at a water–air interface; c and d show silver and 40 nm Au nanoparticle films formed at a water–hexane interface. Silver nanoparticle

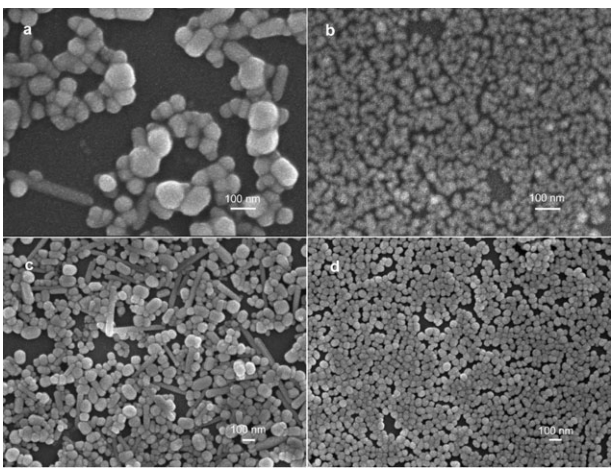

Fig. 3 SEM images of nanoparticle films. (a) and (b): Silver and 12 nm gold nanoparticle films, respectively, formed at a water–air interface. (c) and (d): Silver and 40 nm gold nanoparticle films, respectively, formed at a water–hexane interface.

films formed at the water–air interface showed a network structure (Fig. 3a), whereas films of 12 nm (Fig. 3b) and 40 nm Au nanoparticles (image not shown) usually showed a closely-packed monolayer structure. The nanoparticle films formed at a water–oil interface were usually closely packed with 100–200 nm voids for both gold and silver nanoparticles (Fig. 3c and d), as reported previously.[21,22] We also observed that rapid addition of ethanol formed small aggregates in the monolayer nanoparticle films (Fig. 3c), and addition of too much ethanol led to folding of the nanoparticle films (image not shown). The rate of ethanol addition and the amount added could thus be used to control the structure of the final films. Further experiments showed that the self-assembly of nanoparticles did not depend solely on the particular physicochemical properties of ethanol and hexane. Other organic solvents (*e.g.* methanol, acetone and isopropanol) were also effective for driving the silver and gold nanoparticles to the water–air and water–oil interfaces. In addition, it was found that hexane could be replaced by pentane, cyclohexane or toluene.

In addition to salt-[19] and organic solvent-mediated nanoparticle assembly, most reported methods enable the assembly *via* manipulation of particle hydrophobicity, by coating the nanoparticles with hydrophobic molecules that bind strongly or weakly to their surfaces.[12–18] The importance of a hydrophobic coating in relation to nanoparticle assembly/adsorption was experimentally confirmed by Ramanath and co-workers.[14] They found that agitation of a mixture of $NaBH_4$-reduced gold colloids and toluene resulted in networks of gold nanowires forming at the interface. However, for citrate-reduced gold nanoparticles, the networks of gold nanowires were not observed because the increase in particle hydrophobicity caused by adsorbing toluene was inhibited by strong binding of $C_6H_8O_7^-$ ions to the nanoparticle surfaces. We observed that if silver and gold nanoparticles were first coated with a hydrophilic layer of mercaptoacetic acids, it was difficult to cause them to move to the water–air and water–oil interfaces by subsequent addition of organic solvents. Rao *et al.* found that films already formed at the interface could be re-dispersed to yield either a hydrosol or an organosol with the help of mercaptoundecanoic acid or dodecane thiol.[6] A reasonable conclusion from these experimental observations is that particle hydrophobicity governs both the adsorption of nanoparticles and their stability at interfaces. The following section discusses thermodynamic and kinetic factors governing nanoparticle adsorption, both of which will be seen as closely related to particle hydrophobicity. The basic principles are then used to understand the hydrophobic coating- and organic solvent-mediated self-assembly of nanoparticles.

Thermodynamic and kinetic assesments of nanoparticle adsorption at an interface

Lyophobic colloids are thermodynamically unstable because coagulation results in reduction in thermodynamic "free" energy, but they are kinetically stable. In terms of the Derjaguin–Landau–Vervey–Overbeek (DLVO) theory, this kinetic stability is a consequence of a force barrier that is the sum of the attractive van der Waals force and the repulsive

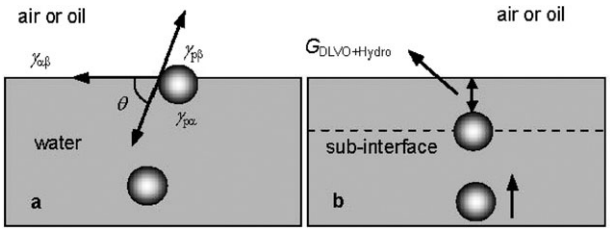

Fig. 4 Schematic model used for (a) thermodynamic evaluation of change in Gibbs free energy before and after moving a particle to the interface; (b) revealing the interactions controlling particle adsorption.

electrostatic force (DLVO interactions) between particles in a dispersion. The force barrier inhibits particle collisions and subsequent coagulation.[29] Because the present assembly is realized *via* destabilization of colloids, it should have a close relationship to colloid stability in solutions. This relationship motivated the treatment of nanoparticle adsorption from both thermodynamic and kinetic viewpoints.

Fig. 4a depicts the position of a spherical particle before and after its adsorption at an interface, from which a change in Gibbs free energy of the colloidal system is evaluated by [30]

$$\Delta E = -\pi r^2 \gamma_{\alpha\beta}(\cos\theta \pm 1)^2$$

where θ is the contact angle measured from the aqueous phase (α), r is particle radius and $\gamma_{\alpha\beta}$ is the interfacial tension. The negative sign in the bracketed term is associated with moving the particle from the α phase to the interface, while the positive sign is associated with moving the particle from the β phase to the interface. ΔE is always negative, so that the Gibbs free energy is reduced by moving the particle to the interface. Consequently, nanoparticle adsorption at the interface is thermodynamically favored whether the particle is hydrophobic or hydrophilic. Conversely, once a particle is trapped at the interface it requires at least a detachment energy $\Delta E' = -\Delta E$, to desorb the trapped particle into the bulk phase. The larger $\Delta E'$ is, the stronger the interfacial trapping. The three parameters r, $\gamma_{\alpha\beta}$, and θ, especially r and θ because $\Delta E'$ is proportional to both r^2 and $(\cos\theta \pm 1)^2$, can be used to control particle stability at the interface. For that reason Rao *et al.* were able to re-disperse nanoparticle films, formed at an interface, into an aqueous or oil phase with the aid of appropriate surfactants to change particle hydrophobicity.[6] Experimental results have proved that to prevent thermally-activated particle desorption $\Delta E'$ should be at least 5–10 times larger than the thermal energy $k_B T$, where k_B is the Boltzmann constant and T is the temperature.[11] This strong interfacial trapping constitutes the basis for trapping and self-assembly of nanoparticles at fluid interfaces.

Although nanoparticle adsorption at the interface is thermodynamically favored, it usually does not occur. This fact strongly indicates that a sorption potential barrier, like the DLVO potential barrier against particle coagulation in a bulk dispersion, kinetically inhibits particle adsorption. Fig. 4b is a schematic adsorption model for elucidating the kinetic factors governing nanoparticle adsorption. As for surfactant adsorption at a solution–air interface,[31] we envisage nanoparticle adsorption as a two-step process. The first step is concentration gradient-driven diffusion of nanoparticles from the bulk phase to the sub-interface, where the interactions between the interface and the adsorbing particles start to take effect. The second step is transport of nanoparticles from the sub-interface to the interface, *i.e.* adsorption. The sorption barrier makes the rate of the adsorption step much smaller than the rate of the diffusion step, so that the overall nanoparticle adsorption process is usually kinetically controlled. To successfully mediate nanoparticle adsorption, it is highly desirable to obtain detailed knowledge of the interactions determining the sorption barrier. Experimental and theoretical studies have revealed that hydrophobic interfaces such as air and oil in contact with water acquire a net negative charge due to accumulation of OH^- at the interfaces at pH > 3–4.[32–36] In such cases, the electrostatic interaction between negatively charged particles and the interface is repulsive. The van der Waals interaction can be either attractive or repulsive, depending on the effective Hamaker constant. Consider the present asymetric interaction, *i.e.*, partice 1 interacts with air (or oil) 2 across medium water 3. The effective Hamaker constant for the van der Waals interaction is $A_{132} = (\sqrt{A_{11}} - \sqrt{A_{33}})(\sqrt{A_{22}} - \sqrt{A_{33}})$, where A_{ii} (i = 1–3) is the Hamaker constant for material i interacting with itself in vacuum. A_{132} is negative because of $A_{11} > A_{33} > A_{22}$, and thus a repulsive van der Waals interaction is predicted. (For usual symmetric interaction, *i.e.*, 1 and 2 are of the same material, $A_{131} = (\sqrt{A_{11}} - \sqrt{A_{33}})^2$ is always positive, and thus van der Waals interaction is always one of attraction.) The electrostatic interaction and the van der Waals interaction are both repulsive, thus the DLVO interactions impose an infinite sorption barrier to particle adsorption.[37] This DLVO explanation obviously conflicts with experimental observations. In previous papers[19,38], a long-range attractive particle-interface force, the hydrophobic force, was proposed to account for particle adsorption. The hydrophobic force and the DLVO interactions cooperatively creates a finite sorption barrier. Particle adsorption occurs when the thermal energy of a particle in the vicinity of the sub-interface exceeds the sorption barrier. This kinetic understanding provides the basis for mediating nanoparticle adsorption and assembly by decreasing the sorption barrier, and increasing the particle kinetic energy by external parameters. The latter effect may account for the observation of Jin *et al.*[20] and other authors[39] that heating can facilitate the assembly of nanoparticles and microparticles at fluid interfaces.

In the adsorption step, the particle starts to interact with the flat air or oil surface across a water medium. The functions for calculating DLVO interactions are well-developed.[40] The hydrophobic force is evaluated by use of the empirical formula proposed by Yoon *et al.*,[41] which we[19] and Schäfer *et al.*[42] have utilized to elucidate silver particle and bacteria accumulation at a water–air interface. The correlation of an attractive force with a high contact angle led to characterization of the force as "hydrophobic force".[43] It exists when one or both of the two interacting surfaces are hydrophobic, and plays an important role in froth flotation.[44] Although its origins are still under debate, by the end of the 20th century it had become accepted as a fundamentally new and important

force.[45] For a spherical particle with radius r, the hydrophobic energy G_{hydro} as a function of distance h from a flat air and/or oil surface is[41]

$$G_{hydro}(h) = -\frac{K_{132}r}{h} \quad (1)$$

where K_{132} is the force constant for particle 1 interacting with air (or oil) 2 across medium 3. K_{132} is uniquely determined by contact angles of the two dissimilar surfaces[41]

$$\log K_{132} = a\left(\frac{\cos\theta + \cos\theta_0}{2}\right) + b \quad (2)$$

where θ is the water contact angle of a particle and θ_0 is the water contact angle of air (or oil). The contact angle of the air (or oil) surface is set at 180° due to its extremely hydrophobic nature.[42] The constants a and b are system specific, and we chose the values $a = -8.2$ and $b = -20$ on the basis of our experimental observations. Finally, a quasi-quantitative equation for the sorption barrier incorporating the particle contact angle is obtained by combining the DLVO interactions and the hydrophobic interaction

$$G_{DLVO+hydro} = G_{DLVO}(h) + G_{hydro}(\theta,h) \quad (3)$$

In our previous paper, we revealed that electrolyte largely decreased the sorption barrier *via* screening the repulsive electrostatic interaction in the DLVO interactions, leading nanoparticle adsorption and subsequent self-assembly of silver nanoparticles at the water–air interface.[19] It is apparent that particle hydrophobicity should also have a large influence on nanoparticle adsorption. In the following two sections, the sorption barrier between a water–air interface and a silver nanoparticle with radius $r = 50$ nm is calculated to illustrate the influence of hydrophobic coatings and organic solvents. In principle, the calculation can be extended to the water–oil system because both oil and air behave as extremely hydrophobic surfaces. In addition, nanoparticle adsorption is not correlated with specific physicochemical properties of the oil phase. Accordingly, air may be viewed as a special type of oil phase, and they function similarly.

Hydrophobic coating-mediated nanoparticle adsorption

Fig. 5 shows calculated sorption barriers encountered when a silver particle with variable hydrophobicity approaches a water–air interface. Parameters of $\zeta_1 = -65$ mV for the water–air interface taken from ref. 33, measured $\zeta_2 = -45$ mV for the silver particle, and $c = 0.1$ mM for electrolyte concentration were used to evaluate the electrostatic interactions. Hamaker constant $A_{132} = -20.7\ k_BT$ was used for evaluating van der Waals energy.[19] Adjustable particle contact angle, which represents the hydrophobicity after surface coating by different surfactants, was used for evaluation of the hydrophobic force. To elucidate the importance of a hydrophobic coating, the repulsive DLVO interactions are assumed not to be affected by a hydrophobic coating, and are kept constant. The calculations thus have two variables, *viz*. particle contact angle θ and particle–interface distance h, and are intentionally applicable to relatively large, repulsive DLVO interactions. It should be noted that modifying a charged particle surface with neutral molecules may reduce surface charges to some extent, which would no doubt further promote particle adsorption and self-assembly.

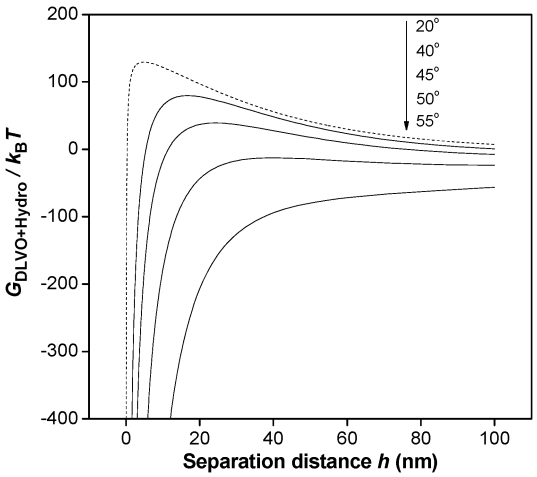

Fig. 5 Sorption barrier between a silver particle ($r = 50$ nm) with varying particle hydrophobicity and a water–air interface.

The solid curves represent the cases in which particle hydrophobicity is gradually increased *via* hydrophobic coating. A rapid decrease in the sorption barrier is observed, because the attractive force represented by $G_{hydro}(\theta,h)$ is sensitively determined by particle hydrophobicity (see eqn (2) for the force constant K_{132}). A small increase in particle contact angle results in a large increase in $G_{hydro}(\theta,h)$. As particle hydrophobicity increases, $G_{hydro}(\theta,h)$ gradually counteracts the repulsive term $G_{DLVO}(h)$, the sorption barrier decreases, and particle adsorption occurs. This sensitive dependence of $G_{hydro}(\theta,h)$ on particle hydrophobicity makes hydrophobic coating a feasible route to mediation of adsorption and self-assembly of nanoparticles.

This choice has been made in reported works, but its role was not fully understood.[12–18] The dashed curve in Fig. 5 represents the calculated sorption barrier when a hydrophilic particle with $\theta = 20°$ approaches the interface. The calculation predicts a high sorption barrier, and hence adsorption of hydrophilic particles is kinetically disfavored. From a thermodynamic point of view, adsorption of a hydrophilic particle is only weakly energy-favored, because the decrease in Gibbs free energy ΔE ($\approx -5k_BT$, evaluated using the values of $r = 50$ nm, $\gamma_{\alpha\beta} = 72$ mN m^{-1}, and $\theta = 20°$) is small and easily allows thermally-activated particle desorption. Consequently, we observed that it was difficult to induce movement of mercaptoacetic acid-modified silver and gold nanoparticles to water–air and water–oil interfaces.

Organic solvent-mediated nanoparticle adsorption

To gain insight into the effect of organic solvents, we need to determine their influence on both $G_{hydro}(\theta,h)$ and $G_{DLVO}(h)$ forces, because all three forces operate across the medium, and the properties of the medium are changed by the addition of organic solvents.

$G_{hydro}(\theta,h)$ is hydrophobicity-dependent, its variation can thus be determined *via* contact angle measurements.[41,43] We used evaporated Ag and Au films to approximately mimic the surface chemistry of silver and Au nanoparticles to reveal the

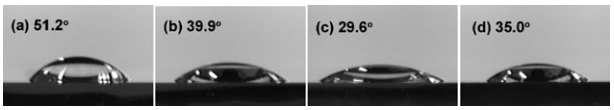

Fig. 6 Photographs of 5 μL water drops on vacuum-evaporated silver films without (a), and with 28.6 vol.% of (b) methanol, (c) ethanol (c), and (d) acetone.

influence trend of organic solvents on the hydrophobic properties of the nanoparticles. It should be noted that at best this can serve as a rough guideline for the trends, not as a precise measurement of the particle contact angle. Fig. 6 shows digital photographs of 5 μL water drops on vacuum-evaporated silver films with and without 28.6 vol.% of organic solvent. A water drop containing 28.6 vol.% of isopropanol spreads on the Ag film, and its photograph is consequently not shown in Fig. 6. The four organic solvents all caused a decrease in the contact angle on vacuum-evaporated Ag films (see ESI for Au films†). According to eqn (2) for the force constant K_{132}, the decrease in particle contact angle caused by addition of organic solvent should lead to a decrease in $G_{\mathrm{hydro}}(\theta,h)$. Kokkoli *et al.* have experimentally observed this co-solvent induced reduction in the hydrophobic force.[46]

The variation in the electrostatic interaction can be confirmed by ζ potential measurements on the silver and gold nanoparticle surfaces. Fig. 7 shows the ζ potentials of silver and 40 nm gold nanoparticles in a water–ethanol medium, as a function of the composition of the medium. The data were corrected for the changes in dielectric constant and viscosity associated with addition of ethanol to water: the details of zeta potential correction and experimental results for other organic solvents can be found in the ESI.†) Compared with the colloids in pure water, addition of ethanol and other organic solvents does not cause a large increase or decrease in zeta potential. This observation is consistent with those of Rubio-Hernández *et al.*[47a] and Odriozola *et al.*[47b] They reported that in general large absolute values of the ζ potential for 638 nm polystyrene particles were observed for small alcohol volume fractions, whereas smaller ζ potential absolute values were seen for large alcohol volume fractions. However, Reincke *et al.* reported gradually decreasing ζ potential with

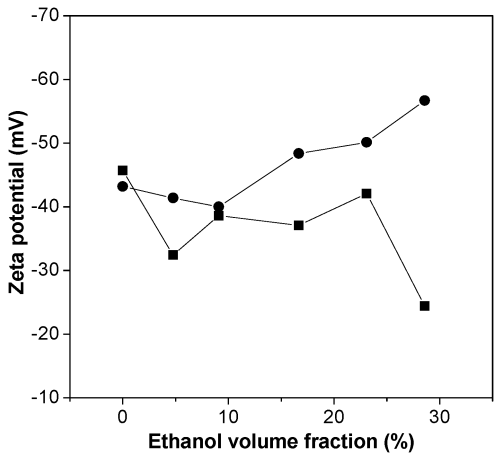

Fig. 7 ζ potentials of silver (■) and 40 nm gold colloids (●) in a water–ethanol medium, as a function of the ethanol volume fraction.

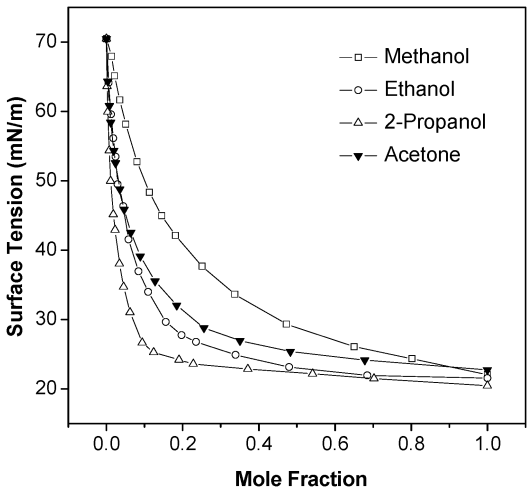

Fig. 8 Surface tension of aqueous solutions of organic solvents as a function of organic solvent mole fraction.

addition of ethanol to citrate-reduced aqueous 4.5 and 16 nm Au colloids. They concluded that reduction of the surface charges on gold nanoparticles, which may be due to binding of ethanol, led to controlled assembly of Au nanoparticles at the water–oil interface.[21] From the adsorption point of view, it is difficult to understand that weak binding of neutral ethanol to nanoparticle surfaces successfully competes with strong binding of citrate ions to the nanoparticles.

We now turn our attention to the other surfaces involved in the electrostatic interaction, *i.e.* the water–air and water–oil interfaces. Fig. 8 shows the results of surface tension measurements. With increasing proportion of organic solvent, the surface tension, γ, of the water–air interface gradually decreases, indicating that the four organic solvents are surface active. In view of the Gibbs adsorption equation,

$$\Gamma = -\frac{a}{RT}\left(\frac{\partial\gamma}{\partial a}\right)_T$$

where Γ is the surface excess concentration of adsorbate and a is the activity of the adsorbate, these organic solvents positively adsorb at the water–air interface. Because the charging mechanism of the water–air interface is accumulation of OH^-,[32–34,36] adsorption of neutral surface active solvents should easily disperse the charge at the interface, as has been confirmed by Takahashi's ζ potential experiments on microbubbles in aqueous solutions.[33] This conclusion can be reasonably extended to the water–oil interface because of its similar charging mechanism[35,36] and the similar enrichment–adsorption of surface active solvents. Thus, the electrostatic interaction also decreases with addition of organic solvents, *via* a "charge dilution" mechanism, due to the positive adsorption of the organic solvents at the charged fluid interface.

Close inspection indicates that the height of the sorption barrier is determined mainly by the attractive $G_{\mathrm{hydro}}(\theta,h)$ term and the repulsive electrostatic force. Therefore, variation in the repulsive van der Waals force with addition of organic solvent has been reasonably neglected. Fig. 9 shows the calculated sorption barrier. To evaluate $G_{\mathrm{hydro}}(\theta,h)$, the contact angle of the silver particle was set at 25° for all

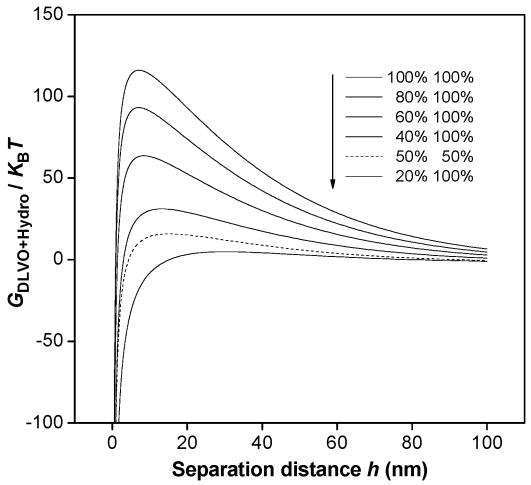

Fig. 9 Sorption barrier between a silver particle (r = 50 nm) and a water–air interface with varying ζ potential values. The dashed curve (50%, 50%) was calculated by decreasing ζ_1 and ζ_2 to half of their original values (*viz.* ζ_1 = −65 mV and ζ_2 = −45 mV).

calculations, which takes account of the reduction in particle hydrophobicity caused by the addition of the organic solvent. This contact angle leads to a three-fold decrease of $G_{hydro}(\theta,h)$ compared with the pure water contact angle (the contact angle of a silver particle in contact with pure water medium is 40° [48]). In parallel, we gradually reduced the ζ potential of the interface (ζ_1 = −65 mV for pure water–air interface[33]) to take into account organic solvent-induced reduction of surface charges, and (on the basis of our ζ potential experiments) keep the ζ potential of the silver nanoparticle (ζ_2 = −45 mV) constant to evaluate the electrostatic interaction at electrolyte concentration c = 1 mM. The solid curves represent the calculated results, which show that the sorption barrier gradually decreases with decrease of the ζ potential of the water–air interface. If the ζ potential of the silver particle is also decreased, the sorption barrier is decreased to a greater extent as illustrated by the dashed curve. These calculations show that even though the attractive hydrophobic force is decreased three-fold, the sorption barrier decreases substantially or eventually disappears if the repulsive electrostatic force can be reduced to a larger extent by addition of organic solvents.

Once the sorption barrier vanishes, nanoparticle adsorption kinetics changes from the usual kinetics-control to diffusion-control. According to the Einstein–Stokes relation, $D = k_BT/6\pi\eta r$, where D is diffusion coefficient and η is the viscosity of the medium, for a nanoparticle with radius r = 50 nm to diffuse vertically a macro distance (*e.g.* 1 mm) in water (η = 0.8937 cP at 298.15 K) takes about 28 h ($t = \bar{x}^2/2D$). This diffusion time is comparable to the time of a few days required for salt-mediated assembly of large scale silver particle films,[19] but is much longer than the time required for an organic solvent-mediated assembly of gold and silver nanoparticles. We believe that agitation from rapid addition of organic solvents to the colloid–air and colloid–oil systems accelerates nanoparticle transport. Since the organic solvents that were used are soluble in water and in the oils, rapid addition of the solvents to a water–oil system produces a flux of solvent across the interface. It is likely that the solvent flux is another cause of the reduction in the time frame for nanoparticle film formation even during the addition of organic solvent for a water–oil interface. Clearly, however, more work is needed to achieve a quantitative understanding of the kinetics of adsorption.

Conclusions

In summary, nanoparticle adsorption at water–air and water–oil interfaces is thermodynamically driven because of the reduction in Gibbs free energy, which results in a deep potential well for strongly trapping nanoparticles at the interfaces and for self-assembly of nanoparticles. However, a finite sorption barrier, which is determined by repulsive DLVO interactions and by the attractive hydrophobic interaction between the interfaces and the adsorbing nanoparticles, kinetically restrains adsorption. A hydrophobic coating changes nanoparticle hydrophobicity and increases the attractive hydrophobic force. Methanol, ethanol, isopropanol, and acetone decrease the attractive hydrophobic force, possibly *via* a solvent effect. However, these neutral organic solvents are surface-active; their positive adsorption at the interface dilutes the charges on the interface and thus decreases the repulsive electrostatic force to a larger extent than the attractive hydrophobic force. Hydrophobic coatings and surface active solvents are thus very effective for manipulation of the interactions determining the sorption barrier, and are hence effective mediators for inducing self-assembly of nanoparticles. We expect this understanding to be of value for the construction of desired nanostructures from diverse colloids at liquid–air and liquid–liquid interfaces.

Acknowledgements

This study was financially supported by Hunan Provincial Natural Science Foundation of China (06JJ3006), Natural Science Foundation of China (20603008, 20703016, and 20873037), and the "985" Foundation of the Ministry of Education of China. We thank Prof. Shuming Nie for helpful discussion and Prof. Bin Ren for improving the English.

References

1 (*a*) D. V. Talapin, E. V. Shevchenko, C. B. Murray, A. Kornowski, S. Förster and H. Weller, *J. Am. Chem. Soc.*, 2004, **126**, 12984–12988; (*b*) J. J. Urban, D. V. Talapin, E. V. Shevchenko and C. B. Murray, *J. Am. Chem. Soc.*, 2006, **128**, 3248–3255.
2 W. H. Binder, *Angew. Chem., Int. Ed.*, 2005, **44**, 5172–5175.
3 D. Wang, H. Duan and H. Möhwald, *Soft Matter*, 2005, **1**, 412–416.
4 D. Yogev and S. Efrima, *J. Phys. Chem.*, 1988, **92**, 5754–5760.
5 A. Berman, N. Belman and Y. Golan, *Langmuir*, 2003, **19**, 10962–10966.
6 C. N. R. Rao, G. U. Kulkarni, P. J. Thomas, V. V. Agrawal and P. Saravanan, *J. Phys. Chem. B*, 2003, **107**, 7391–7395.
7 C. Collier, T. Vossmeyer and J. Heath, *Annu. Rev. Phys. Chem.*, 1998, **49**, 371–404.
8 K. S. Mayya and M. Sastry, *Langmuir*, 1999, **15**, 1902–1904.
9 D. Wyrwa, N. Beyer and G. Schmid, *Nano Lett.*, 2002, **2**, 419–421.
10 B. Su, J.-P. Abid, D. J. Fermin, H. H. Girault, H. Hoffmannová, P. Krtil and Z. Samec, *J. Am. Chem. Soc.*, 2004, **126**, 915–919.

11 (*a*) Y. Lin, H. Skaff, T. Emrick, A. D. Dinsmore and T. P. Russell, *Science*, 2003, **299**, 226–229; (*b*) Y. Lin, H. Skaff, T. Emrick, A. Böker, A. D. Dinsmore, T. Emrick and T. P. Russell, *J. Am. Chem. Soc.*, 2003, **125**, 12690–12691; (*c*) Y. Lin, A. Böker, H. Skaff, D. Cookson, A. D. Dinsmore, T. Emrick and T. P. Russell, *Langmuir*, 2005, **21**, 191–194.
12 L. L. Dai, R. Sharma and C.-Y. Wu, *Langmuir*, 2005, **21**, 2641–2643.
13 A. Kumar, S. Mandal, S. P. Mathew, P. R. Selvakannan, A. B. Mandale, R. V. Chaudhari and M. Sastry, *Langmuir*, 2002, **18**, 6478–6483.
14 G. Ramanath, J. D'Arcy-Gall, T. Maddanimath, A. V. Ellis, P. G. Ganesan, R. Goswami, A. Kumar and K. Vijayamohanan, *Langmuir*, 2004, **20**, 5583–5587.
15 B. Kim, S. L. Tripp and A. Wei, *J. Am. Chem. Soc.*, 2001, **123**, 7955–7956.
16 I. Šloufová-Srnová and B. Vlčková, *Nano Lett.*, 2002, **2**, 121–125.
17 H. Duan, D. Wang, D. G. Kurth and H. Möhwald, *Angew. Chem., Int. Ed.*, 2004, **43**, 5639–5642.
18 S. Yamamoto and H. Watarai, *Langmuir*, 2006, **22**, 6562–6569.
19 J.-W. Hu, G.-B. Han, B. Ren, S.-G. Sun and Z.-Q. Tian, *Langmuir*, 2004, **20**, 8831–8838.
20 Y. Jin and S. Dong, *Angew. Chem., Int. Ed.*, 2002, **41**, 1040–1044.
21 F. Reincke, S. G. Hickey, W. K. Kegel and D. Vanmackelbergh, *Angew. Chem., Int. Ed.*, 2004, **43**, 458–462.
22 Y.-J. Li, W.-J. Huang and S.-G. Sun, *Angew. Chem., Int. Ed.*, 2006, **45**, 2537–2539.
23 L. Huo, W. Li, L. Lu, H. Cui, S. Xi, J. Wang, B. Zhao, Y. Shen and Z. Lu, *Chem. Mater.*, 2000, **12**, 790–794.
24 V. N. Paunov, B. P. Binks and N. P. Ashby, *Langmuir*, 2002, **18**, 6946–6855.
25 F. Reincke, W. K. Kegel, H. Zhang, M. Nolte, D. Wang, D. Vanmaekelbergh and H. Möhwald, *Phys. Chem. Chem. Phys.*, 2006, **8**, 3828–3835.
26 (*a*) R. Aveyard, J. H. Clint, D. Nees and V. N. Paunov, *Langmuir*, 2000, **16**, 1969–1246; (*b*) R. Aveyard, B. P. Binks, J. H. Clint, P. D. I. Fletcher, T. S. Horozov, B. Neumann and V. N. Paunov, *Phys. Rev. Lett.*, 2002, **88**, 246102–1; (*c*) F. Martínez-López, M. A. Cabrerizo-Vílchez and R. Hidalgo-Álvarez1, *J. Colloid Interface Sci.*, 2000, **232**, 303–310; (*d*) J. C. Fernández-Toledano, A. Moncho-Jordá, F. Martínez-López and R. Hidalgo-Álvarez1, *Langmuir*, 2004, **20**, 6977–6980; (*e*) J. C. Fernández-Toledano, A. Moncho-Jordá, F. Martínez-López and R. Hidalgo-Álvarez1, *Langmuir*, 2006, **22**, 6746–6749; (*f*) S. Reynaert, P. Moldenaers and J. Vermant, *Langmuir*, 2006, **22**, 4936–4945; (*g*) S. Reynaert, P. Moldenaers and J. Vermant, *Phys. Chem. Chem. Phys.*, 2007, **9**, 6463–6475; (*h*) B. J. Park, J. P. Pantina, E. M. Furst, M. Oettel, S. Reynaert and J. Vermant, *Langmuir*, 2008, **24**, 1686–1694.
27 P. C. Lee and D. Meisel, *J. Phys. Chem.*, 1982, **86**, 3391–3395.
28 G. Frens, *Nat. Phys. Sci.*, 1973, **241**, 20–22.
29 P. C. Hiemenz and R. Rajagopalan, *Principles of Colloid and Surface Chemistry*, Marcel Dekker, New York, 3rd edn, 1997, p. 575.
30 B. P. Binks, *Curr. Opin. Colloid Interface Sci.*, 2002, **7**, 21–41.
31 J. Liu, C. Yang, C. Zhang and U. Messow, *Colloid Polym. Sci.*, 2005, **284**, 92–96.
32 A. Graciaa, G. Morel, P. Saulner, J. Lachaise and R. S. Schechter, *J. Colloid Interface Sci.*, 1995, **172**, 131–136.
33 M. Takahashi, *J. Phys. Chem. B*, 2005, **109**, 21858–21864.
34 P. Creux, J. Lachaise, A. Graciaa and J. K. Beattie, *J. Phys. Chem. C*, 2007, **111**, 3753–3755.
35 J. K. Beattie and A. M. Djerdjev, *Angew. Chem., Int. Ed.*, 2004, **43**, 3568–3571.
36 K. N. Kudin and R. Car, *J. Am. Chem. Soc.*, 2008, **130**, 3915–3919.
37 A. I. Abdel-Fattah and M. S. El-Genk, *Adv. Colloid Interface Sci.*, 1998, **78**, 237–266.
38 D. F. Williams and J. C. Berg, *J. Colloid Interface Sci.*, 1992, **152**, 218–229.
39 S. H. Im, Y. T. Lim, D. J. Suh and O. O. Park, *Adv. Mater.*, 2002, **14**, 1367–1369.
40 W. Norde and J. Lyklema, *Colloids Surf.*, 1989, **38**, 1–13.
41 R. H. Yoon, D. H. Flinn and Y. I. Rabinovich, *J. Colloid Interface Sci.*, 1997, **185**, 363–370.
42 A. Schäfer, H. Harms and A. J. Zehnder, *Environ. Sci. Technol.*, 1998, **32**, 3704–3712.
43 M. Mao, J. Zhang, R.-H. Yoon and W. A. Ducker, *Langmuir*, 2004, **20**, 1843–1849.
44 W. A. Ducker, Z. Xu and J. N. Israelachvili, *Langmuir*, 1994, **10**, 3279–3289.
45 P. Attard, *Adv. Colloid Interface Sci.*, 2003, **104**, 75–91.
46 E. Kokkoli and C. F. Zukoski, *J. Colloid Interface Sci.*, 1999, **209**, 60–65.
47 (*a*) F. J. Rubio-Hernández, F. J. de las Nieves, R. Hidalgo-Álvarez and B. H. Bijsterbosch, *J. Dispersion Sci. Technol.*, 1994, **15**, 1–19; (*b*) G. Odriozola, A. Schmitt, J. Callejas-Fernández and R. Hidalgo-Álvarez, *J. Colloid Interface Sci.*, 2007, **310**, 471–480.
48 Y.-L. Lee, W.-S. Chou and L.-H. Chen, *Surf. Sci.*, 1998, **414**, 363–373.